Dynamics of Intramural and Transmural Reentry During Ventricular Fibrillation in Isolated Swine Ventricles

Miguel Valderrábano, Moon-Hyoung Lee, Toshihiko Ohara, Angela C. Lai, Michael C. Fishbein, Shien-Fong Lin, Hrayr S. Karagueuzian and Peng-Sheng Chen

Circ Res. 2001;88:839-848; originally published online April 13, 2001;
doi: 10.1161/hh0801.089259
Circulation Research is published by the American Heart Association, 7272 Greenville Avenue, Dallas, TX 75231

Print ISSN: 0009-7330. Online ISSN: 1524-4571

Dynamics of Intramural and Transmural Reentry During Ventricular Fibrillation in Isolated Swine Ventricles

Miguel Valderrábano, Moon-Hyoung Lee, Toshihiko Ohara, Angela C. Lai, Michael C. Fishbein, Shien-Fong Lin, Hrayr S. Karagueuzian, Peng-Sheng Chen

Abstract—The intramural dynamics of ventricular fibrillation (VF) remain poorly understood. Recent investigations have suggested that stable intramural reentry may underlie the mechanisms of VF. We performed optical mapping studies of VF in isolated swine right ventricles (RVs) and left ventricles (LVs). Nine RV walls were cut obliquely in their distal edge exposing the transmural surface. Six LV wedge preparations were also studied. Results showed that intramural reentry was present. In RV, 28 of 44 VF episodes showed reentry; 15% of the activation pathways were reentrant. Except for 4 episodes, reentry was transmural, involving subendocardial structures as the papillary muscle (PM) or trabeculae. In LV, reentry was observed in 27 of 27 VF episodes; 23% of the activations were part of reentrant pathways ($P<0.05$ compared with RV). All LV reentrant pathways were truly intramural (confined to the wall) and were frequently located at the PM insertion. In both ventricles, reentry was spatially and temporally unstable. Histological studies showed abrupt changes in fiber orientation at sites of reentry and wave splitting. Connexin 40 immunostaining demonstrated intramyocardial Purkinje fibers at sites of reentry in the PM root and around endocardial trabeculae. Our results confirm that reentry is frequent—but unstable—in the myocardial wall during VF. In RV, reentry is mostly transmural and requires participation of subendocardial structures. The LV has a greater incidence of reentry and is intramural. Anisotropic anatomic structures played key roles in the generation of wave splitting and in the maintenance of reentry. **(*Circ Res*. 2001;88:839-848.)**

Key Words: intramural reentry ■ fibrillation ■ anisotropy ■ Purkinje ■ papillary muscle

Our current knowledge of the activation dynamics that take place during ventricular fibrillation (VF) derives from multiple endocardial and/or epicardial mapping studies.[1–5] On the basis of these data, VF has been characterized by spatiotemporal heterogeneity because of the coexistence of both organized reentry and fragmented wavelets.[3,4,6,7] However, the intramural dynamics of VF remain largely unexplored because of the lack of an experimental model that allows for intramural mapping of VF. Recent studies[8,9] have suggested that rapid and stable intramural reentry might serve as the source of VF. Intramural reentry has been previously demonstrated during ventricular tachycardia or fibrillation,[1,10–13] but whether stable intramural reentry occurs during VF and to what extent is it required to maintain VF are unanswered questions. We have developed an experimental model to study intramural patterns of activation during VF. Our results confirm that reentry is indeed frequently seen in the myocardial wall. Substantial differences are noted between right ventricle (RV) and left ventricle (LV). We also demonstrate that anatomic structures played key roles in the generation of wave splitting and in the maintenance of reentry.

Materials and Methods

RV Preparation

The experimental model has been previously described.[14] Briefly, the hearts of 9 farm pigs were extracted, and the right coronary artery was perfused. The RV wall was excised and placed in a tissue bath, with the endocardium facing up. An oblique cut was performed at the distal edge, exposing the transmural surface (see online Figure 1 in the data supplement available at http://www.circresaha.org) and including the papillary muscle (PM). Optical mapping (see below) during VF was performed in the cut surface as well as in the adjacent endocardial surface.

LV Preparation

Our LV wedge preparation was similar to that described by the laboratory of Yan et al.[15] In 4 hearts, a rim of tissue surrounding the left circumflex and the second obtuse marginal artery was excised and perfused, leaving an inverted L-shaped preparation that contained at least part of the posteromedial PM. The tissue was placed in the tissue bath with the transmural cut surface up (see online Figure 1). In 2 tissues, the left circumflex artery was ligated

Original received October 27, 2000; resubmission received January 30, 2001; revised resubmission received February 26, 2001; accepted February 26, 2001.

From the Division of Cardiology, Department of Medicine (M.V., M.-H.L, T.O., A.C.L., H.S.K., P.-S.C.), Cedars-Sinai Medical Center, and the Department of Pathology and Anatomy (M.C.F.), UCLA School of Medicine, Los Angeles, Calif, and the Department of Physics and Astronomy (S.-F.L.), Vanderbilt University, Nashville, Tenn.

Correspondence to Peng-Sheng Chen, MD, Room 5342, Cedars-Sinai Medical Center, 8700 Beverly Blvd, Los Angeles, CA 90048. E-mail chenp@csmc.edu

Circulation Research **is available at http://www.circresaha.org**

Characteristics and Frequency of Transmural Reentry in VF

Tissue	VF With Reentry (Total)	Reentry Episodes	Cycles	Reentry Cycle Length, ms	Frequency, Hz	Reentry in PM	Reentry Elsewhere
RV tissues							
1	4	14	7.3±11.9	80.3±5.8	12.4±1.3	9	4
2	1	1	1±0	105.1±0	9.5±0	0	1
3	5	12	2.2±1.6	68.2±5.9	14.7±1.9	4	7
4	1	2	4±0	78.1±8.2	12.8±0.6	2	0
5	1	2	18±0	86.3±10.3	11.6±0.2	1	1
6	5	19	3.3±1.6	74.7±7.9	13.4±1.5	6	8
7	1	2	11±8.5	103.7±2.1	9.7±0.1	2	0
8	4	14	8.5±15.8	58.4±3.8	17.1±0.8	2	11
9	6	16	3.1±1.5	69.1±4.6	14.5±0.7	10	6
Total	28 (44)	82	6.5±5.4	80.4±15.8	12.9±2.4	36	38*
LV tissues							
1	1	3	7.3±6.5	86.5±7.2	11.6±1.9	0	3
2	8	21	7.2±11.1	79.8±6	12.5±1	16	10
3	2	8	5.2±4.3	82.2±9.6	12.2±1.3	0	8
4	4	10	6.3±5.2	81±3	12.3±1	7	3
5	5	22	4.2±3	73.4±4.5	13.6±0.7	17	5
6	7	21	6.1±7.8	78.1±9.2	12.8±1.5	10	6
Total	27 (27)	85	6.1±1.2	80.2±4.4	12.5±0.7	50	35

*In RV, 38 episodes of reentry involved endocardial trabeculae. The remaining 8 episodes (not shown) occurred elsewhere.

proximally and a wedge of tissue surrounding the left anterior descending artery was cut, exposing the transmural surface of the interventricular septum. Tyrode's solution was perfused via the left coronary artery. These 6 LV wedges developed VF during manipulation, which persisted for 63 to 79 minutes.

Optical Mapping

The optical mapping system was similar to the one described previously.[16] The tissues were stained for 20 minutes with 1 to 2 μmol/L di-4-ANEPPS. Quasimonochromatic light (500±30 nm) was shone on the tissues, and the fluorescence was collected through a 600-nm long-pass glass filter with charge-coupled device camera, at ≈279 frames per second, acquiring 96×96 sites simultaneously. Each acquisition lasted for 4.3 seconds.

Data Analysis

The fluorescent signals were processed to reduce the noise.[16] Each pixel was assigned a shade of gray between white (representing a fully depolarized state) and black (representing a fully repolarized state). The activation wavefront was colored red, and the repolarization waveback was colored green. The area between a red and a green line constituted a wavelet. A wavebreak point in a propagating wavelet is a point at which a red line and a green line meet. Wave splitting was defined as the generation of 2 daughter wavelets—and 2 wavebreak points—from a single wavelet. Reentry was defined to be present when a wavefront rotated around a wavebreak point completing a 360° cycle. Reentry was considered intramural when the complete rotation occurred within the wall without invading the adjacent endocardial or epicardial surface. Transmural reentry was defined as that which involved both the myocardial wall and the endocardium or subendocardial structures such as the PM or trabeculae. The fraction of reentrant wavelets was determined by the ratio of the number of wavelets participating in a reentrant circuit over the total number of wavelets in the mapping field.

Data are reported as mean±SD. Linear regression analysis was used to correlate frequencies. A Student *t* test was used to compare means. A χ^2 test was used to compare the proportion of reentrant episodes in LV versus RV and the proportion of reentrant episodes located at the PM. A P value ≤ 0.05 was considered significant.

Sections of 5 μm parallel to the mapped surface were stained with Masson's trichrome. We also used connexin 40 (Cx40) immunostaining[17] to identify intramyocardial Purkinje fibers.

Electrocardiographic and Frequency Analysis

Fast Fourier transformation was performed on signals from the recorded pseudo-ECG and the local fluorescence signals from each pixel of the optical mapping field. The dominant frequency was defined as that with the highest power of each frequency spectrum. Frequency domain maps were constructed as previously reported.[9]

An expanded Materials and Methods section can be found in an online data supplement available at http://www.circresaha.org.

Results

Right Ventricle

A total of 44 VF episodes (4.3 seconds each) were successfully mapped; of these, 28 showed at least 1 episode of reentry (Table). A total of 82 episodes of reentry were identified in these 28 episodes of VF. The fraction of wavelets that participated in a reentrant circuit was 15% (82 of 563 total number of visualized wavelets). Most episodes of reentry were short-lived, with a range of 1 to 47 rotations. Figure 1 shows a histogram with the number of cycles per episode of reentry. The reentry frequencies and cycle lengths are shown in the Table. Different patterns occurred in the same tissue in different VF episodes. Visualization of the raw optical mapping data permitted spatial localization of the sites where reentry occurred. Two episodes of reentry occurred in the mapped endocardial surface, whereas the remaining 80

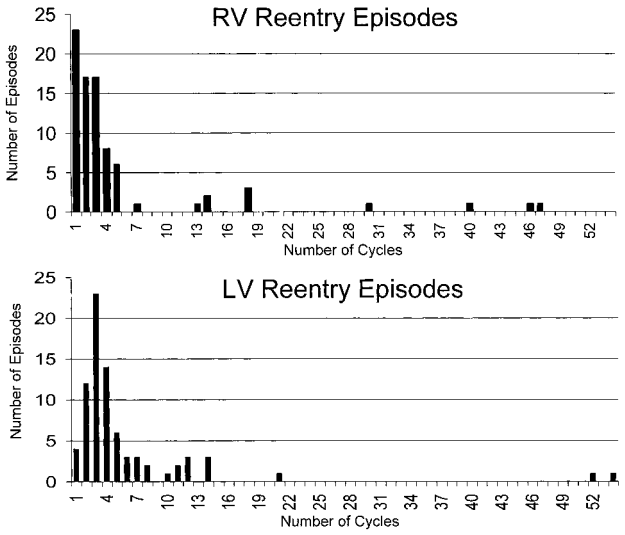

Figure 1. Histograms showing number of cycles per reentry episode.

episodes involved the myocardial wall. In most instances (77 of 80, 96%), reentry in the myocardial wall involved subendocardial structures (namely, the PM insertion or trabeculae), and thus was not truly intramural but rather transmural. This could coexist with intramural reentry (see below) in figure 8 patterns. All of the 10 episodes that lasted >10 rotations (Figure 1) involved reentry localized to the PM or trabeculae.

Intramural Reentry

Four episodes of intramural reentry were observed. Figure 2 shows an example of a figure 8 reentry with 1 intramural loop. In the left upper corner of the tissue, 2 wavelets collided and merged in the endocardial edge of the cut surface in panels A through C. Then, a division occurred at the takeoff of an endocardial trabecula (panels D and E, and panel K for the identification of endocardial trabecula). One wavelet rotated clockwise toward the endocardium, whereas the other did so intramurally in a counterclockwise direction. Panel N shows an isochronal map during 1 rotation. Eighteen rotations were completed.

The remaining 3 episodes of true intramural reentry were isolated and did not involve figure 8 patterns (online Figure 2 in the data supplement [http://www.circresaha.org] shows an example). They persisted for 5, 6, and 8 rotations, respectively.

Transmural Reentry Involving PM and Endocardial Trabecula

Figure 3 shows, in the same tissue as Figure 2, an example of transmural reentry in which both the PM and an endocardial

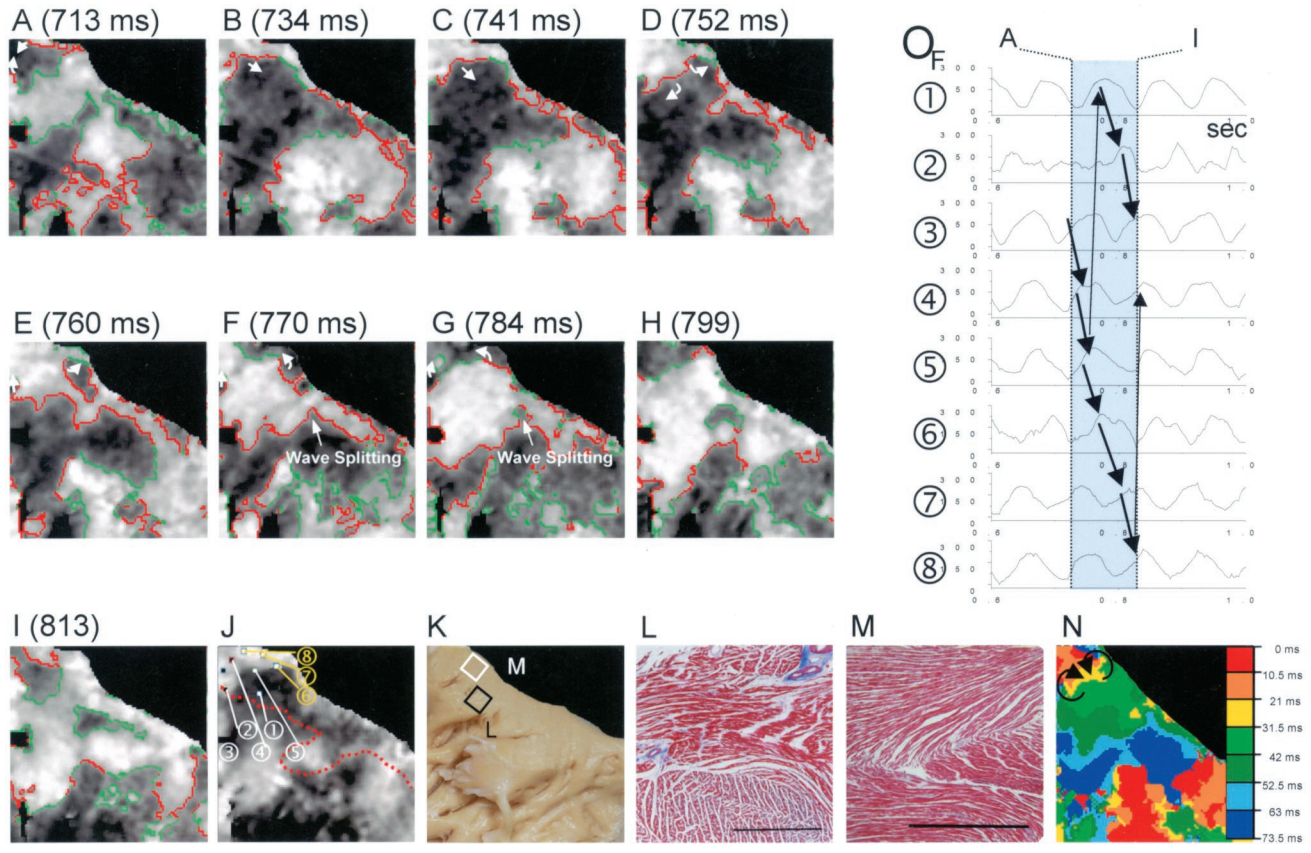

Figure 2. Intramural and transmural reentry in the RV. A through I, Figure 8 reentry; one wavelet rotates counterclockwise intramurally whereas the other uses a trabecula to rotate clockwise in endocardium (arrows). G, Wave splitting at the PM root. J, Location of channels for which optical action potentials are shown in panel O (in fluorescence [F] units). Red dotted line marks the location of the endocardial edge. K, Photograph of tissue showing trabeculae and PM. L, Histology at the site of trabecular insertion (black outline in K). M, Histology at the site of intramural reentry (white outline in K). Bar=1 mm. N, Isochronal map. In panel O, A and I refer to panels A through I. See text for details.

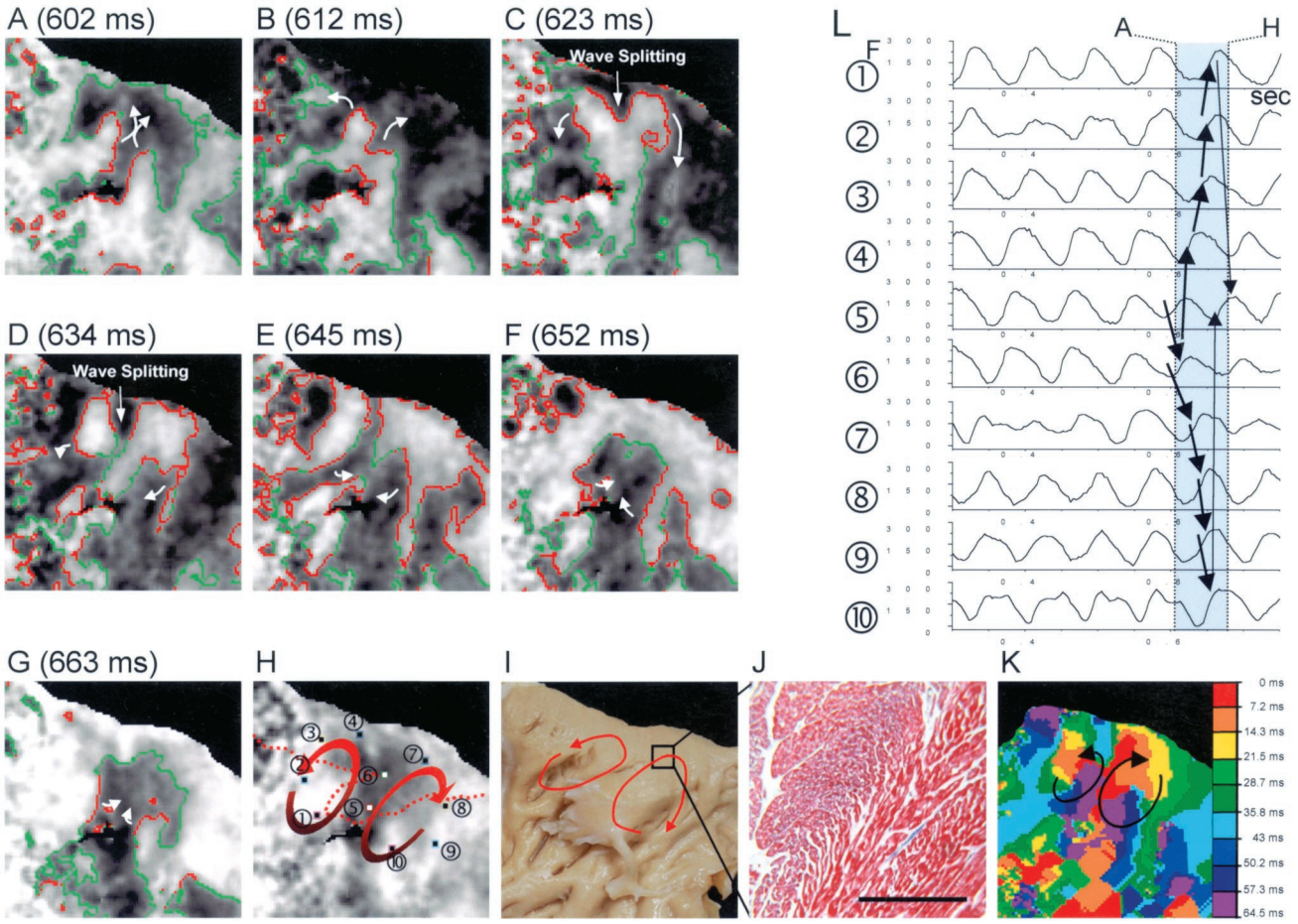

Figure 3. Transmural reentry in the PM root in the RV. A through G, Figure 8 reentry using PM and trabeculae as part of the reentrant pathway (arrows). Wave splitting in PM is shown in panel C. H, Schematic of reentrant circuit, and location of channels for which optical action potentials are shown in panel L. Dotted line shows outline of PM. I, Photograph of tissue showing trabeculae and PM. J, Histology at the site of wave splitting at the PM root. Bar=1 mm. K, Isochronal map. Units as in Figure 2. See text for details.

trabecula participated in the circuit. The dotted line in panel H shows the outline of the PM. In panel A, 2 wavelets invaded the PM, where they eventually merged (panel B). This new wavelet traveled toward the PM root, where it split again (panel C), giving rise to 2 daughter wavelets (panel D). The one on the right turned clockwise and went back in the endocardial surface using an endocardial trabecula as its pathway (panels D, E, and F, and panel I for identification of the trabecula). This wavelet then reentered the PM (panel G). The other wavelet turned counterclockwise and similarly went back to the endocardial surface through a trabecula and then reentered the PM (panels D, E, and F). Panel K shows an isochronal map during 1 rotation. Seven rotations were completed.

Wave Splitting

Wave splitting was more frequent than reentry, and it was consistently localized to underlying anatomic structures; of a total of 154 episodes, 102 (66%) were mapped at the PM root, and 52 (34%) at an endocardial trabecula. Figures 2 and 3 show examples of wave splitting in the same site but with opposite wave directions, along with the fiber orientation patterns at the splitting site (Figure 3).

Left Ventricle

All VF episodes in all 6 tissues showed episodes of reentry (see Table). A total of 85 reentry episodes were mapped in 27 episodes of VF. Relative to the number of VF episodes, reentry was more common in the LV than in the RV (85 reentry episodes in 27 VF episodes versus 82 in 44, $P=0.001$). The fraction of wavelets participating in a reentrant circuit relative to the total number of visualized wavelets was 23% (85 of 373), significantly ($P<0.05$) higher than the fraction of reentrant wavelets in the RV. As in the RV, most of these were unstable and short-lived (see Figure 1), with the number of cycles ranging from 1 to 54. There were no significant differences in reentry frequencies or cycle lengths between RV and LV (Table). All of these episodes of reentry in the LV were true intramural reentry.

Intramural Reentry at the Insertion Site of the PM

Reentry occurred in the root of the PM in 59% (50 out of 85 episodes), a similar proportion as in the RV (36 out of 74 episodes, 49%, P=NS). Figure 4 shows an example of intramural reentry around the PM insertion. The dotted line in panel I shows the outline of the intramural PM root. As shown in panel A, a wavelet approached the PM moving clockwise toward its root. Wave splitting occurred, and 2

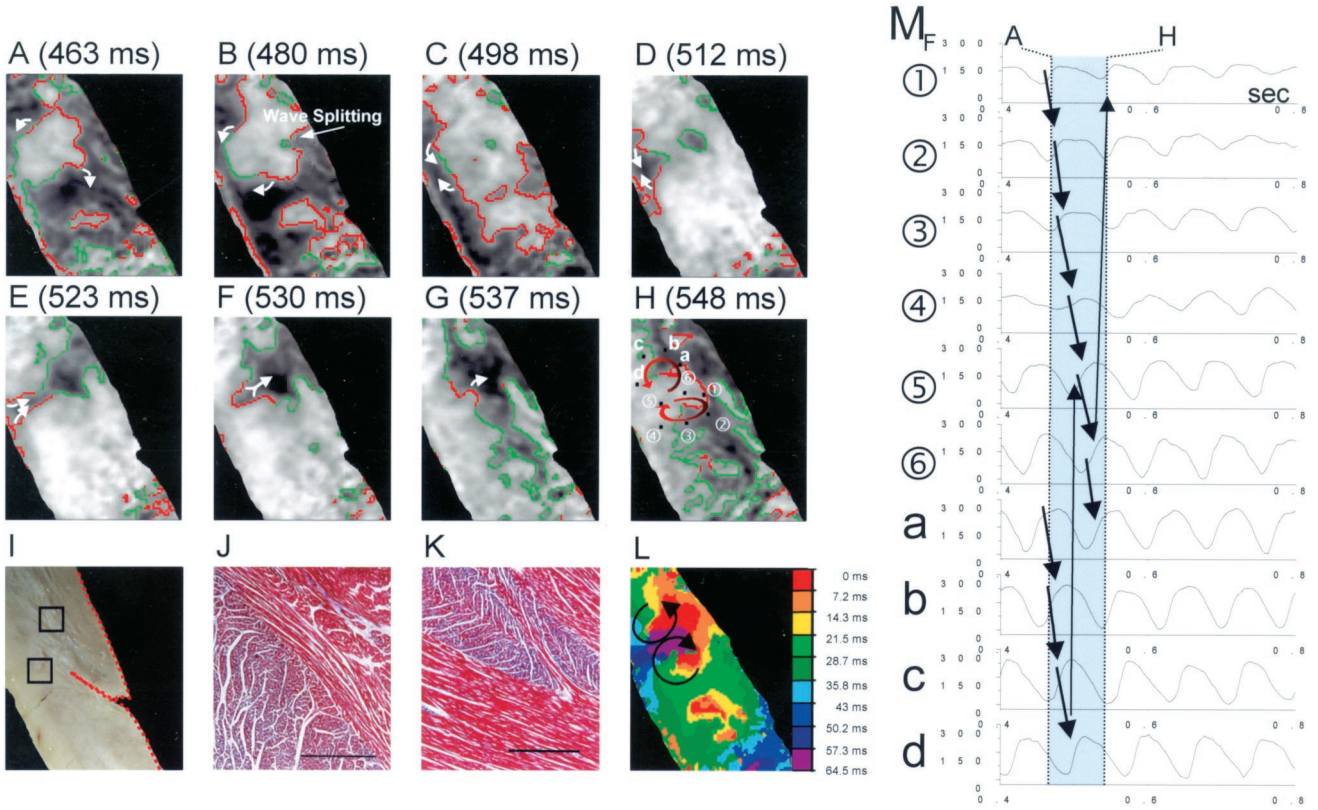

Figure 4. Reentry in PM in the LV. A through H, Figure 8 reentry in the PM root. B, Wave splitting in PM, with generation of 2 wavelets. H, Schematic of reentry and location of channels for which the optical action potentials are shown in panel M. I, Photograph of tissue showing PM (dotted red line). J, Histology at the core of reentry of the bottom wavelet. K, Histology at the site of wave splitting. J and K, Bar=1 mm. L, Isochronal map. Units as in Figure 2. See text for details.

wavelets resulted. The one on the bottom rotated clockwise along the PM root, whereas the one on top did so counterclockwise (panels A through H). They merged again in panel F, and 5 more rotations were completed. Interestingly, the upper loop of the figure 8 pattern was only present in 2 of the 6 total rotations. Panel L shows an isochronal map of this rotation.

Reentry Not Involving PM

Reentry outside the PM root occurred in 41% of the episodes. Most often, the reentry site could not be identified as any particular macroscopic anatomic structure. In 1 episode, reentry occurred around a subepicardial artery that had been ligated.

The septal preparation (N=2) did not include PM but still showed episodes of reentry. Figure 5 shows an example. In the right upper quadrant of the tissue, a wavelet rotated clockwise with the typical appearance of a spiral wave. Panels A through L show the last 2 rotations (of a total of 12) completed by this spiral wave. Before its extinction, this spiral seemed to give rise to all of the other wavelets that activated the tissue. As seen in panel B, a daughter wavelet arose from the spiral, detached from it (panels E and F), and proceeded to activate the bottom portion of the tissue (panels G and H). A second daughter wavelet arose from the side of the spiral (panels D; E; and, in a subsequent rotation, J) that activated the left upper portion of the tissue. In both instances, these daughter wavelets merged with others that arose as breakthrough activations (left upper corner of the tissue in panels F and K) or from nonmapped portions of the tissue (bottom part in panel E). However, the appearance of these other wavelets was, if not physically connected to the ones arising from the spiral, at least chronologically synchronized, given that they always appeared simultaneously. Panel R shows an isochronal map of 1 rotation, suggesting that the wavelets in the left half of the tissue arise from the spiral (dashed arrows). This pattern eventually destabilized. Panels J through O show how the spiral annihilated itself. Up to panel I, the rotation proceeded as previously. As seen in panels I through M, the progression of the wavelet was slowed and took 61 ms to complete the rightmost part of the rotation (a step that in the previous cycle—panels D through F—had only taken 33 ms). This slowing is clearly shown in panel U, in which the activation from channel 6 to channel 1 is delayed (curved arrow). The result is that, as shown in panels K, L, and M, the spiral gave rise to another wavelet (yellow arrows) that collided with the primary one (panels N and O) and interrupted the reentry. Multiple nonreentrant wavelets were seen afterward in this episode.

PM and Wave Splitting

Sixty-eight episodes of wave splitting were mapped. The PM root served as a site of splitting in 52 of them (the rest were due to wave collisions). Figure 4 shows an episode of wave

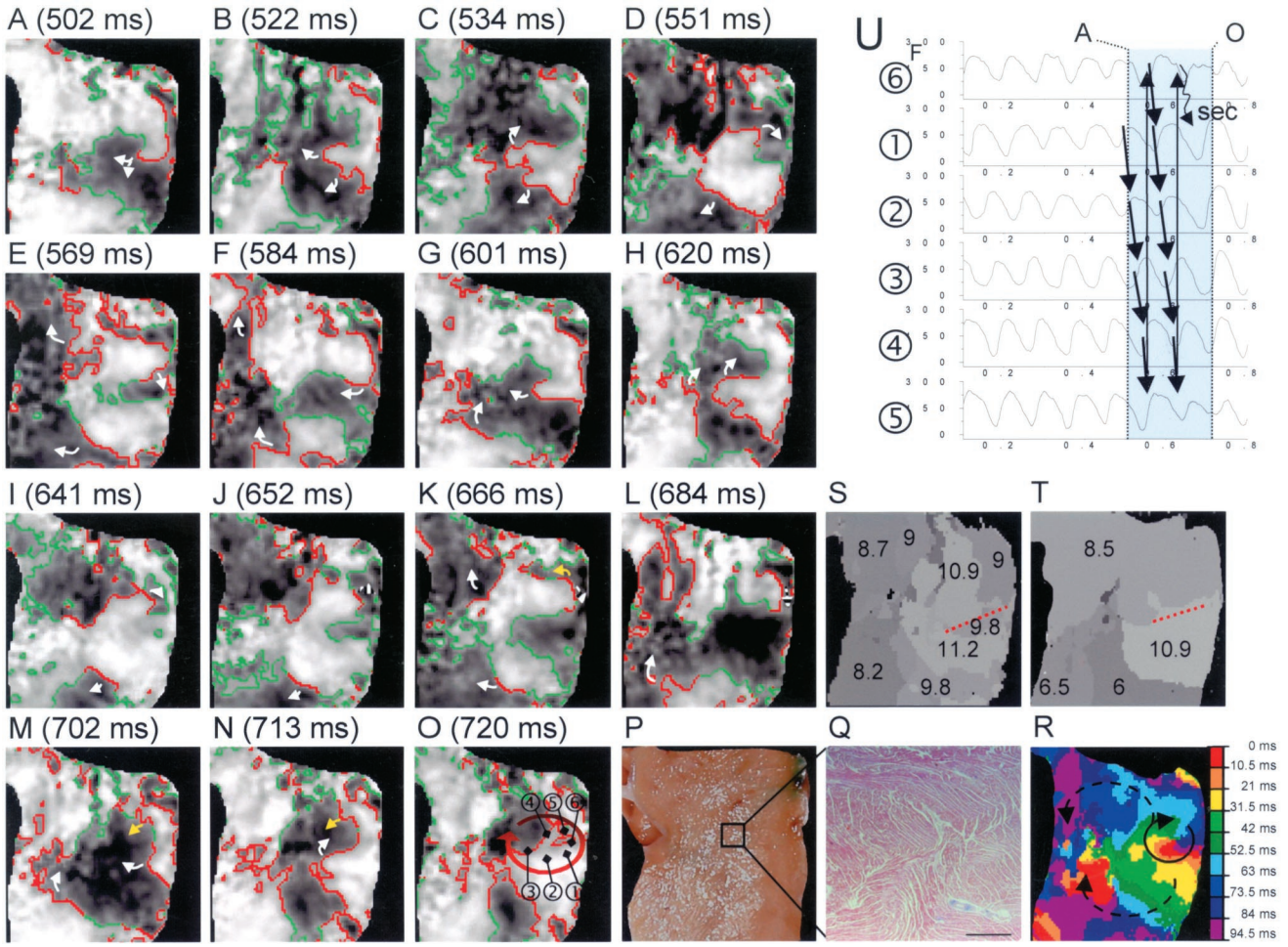

Figure 5. Spiral wave reentry; a possible mother rotor in the LV. A through I, Spiral wave rotates clockwise (white arrows). I through M, Slow conduction of the spiral (dashed arrows). M through O, Spiral annihilation by wave collision. K, L, and M, Spiral gives rise to another wavelet (yellow arrows) that collides with the primary one (N and O) and interrupts reentry. O, Schematic of reentry and location of channels for which optical action potentials are shown in panel U. P, Photograph of tissue showing the site of reentry. Q, Histology at the site of reentry. R, Isochronal map. Bar=1 mm. S, Frequency mapping during the 4.3-second episode that included this reentry (numbers in Hz). T, Frequency mapping during a separate episode. The red dotted lines in S and T are frequency domain boundaries that remain stable in absence of PM. Units as in Figure 2. See text for details.

splitting followed by figure 8 reentry, along with the local histological pattern (panel K).

Anatomic Correlates of Wavelet Behavior: Fiber Orientation and Intramyocardial Purkinje Fibers

Histological analyses were performed with tissue specimens from the mapped surfaces. Similar patterns of complex fiber architecture, with sharp fiber angulations, were found in all of the sites of reentry, both in RV and LV (see Figures 2L, 2M, 3J, 4J, 4K, and 5Q). Transversely cut fibers were seen in juxtaposition with longitudinally cut fibers, thereby potentially creating discrete regions of discontinuous anisotropy. The PM root and the root of endocardial trabecula in the RV consistently exhibited this pattern, but similar convoluted patterns were also found at other sites of reentry, even when these were distant from the trabeculae or the PM (see Figure 5Q).

Wave splitting, with the generation of wavebreak points in a propagating wavelet, was localized in the PM root or in trabeculae in the vast majority of the mapped episodes (93%, 206 of 222 episodes, adding the RV and LV cases). The Purkinje–ventricular muscle junction (PVJ) is known to be a region of low safety factor and potential unidirectional block.[18,19] Because PVJs in the PM are predominantly located at its base,[20] we hypothesized that PMJs could have played a role in the observed findings. Cx40 immunostaining successfully identified intramyocardial Purkinje fibers, which were often indistinct from working myocytes on trichrome staining. These intramyocardial Purkinje fibers ran in 1- or 2-cell columns,[21] separating clearly delimited muscle bundles. Along with abrupt fiber orientation changes, both the PM root and the endocardial trabeculae in the RV were remarkable for the presence of intramyocardial Purkinje fibers that separated them from neighboring myocardial muscle bundles. This bundle separation was prominent in the case of endocardial trabeculae in the RV (see online Figure 3 in the data supplement [http://www.circresaha.org]). In the PM, Purkinje fibers were located at the root, where single-cell PMJs were present (Figure 6).

The association between anisotropy, intramyocardial Purkinje fiber location, and wavelet behavior was not completely

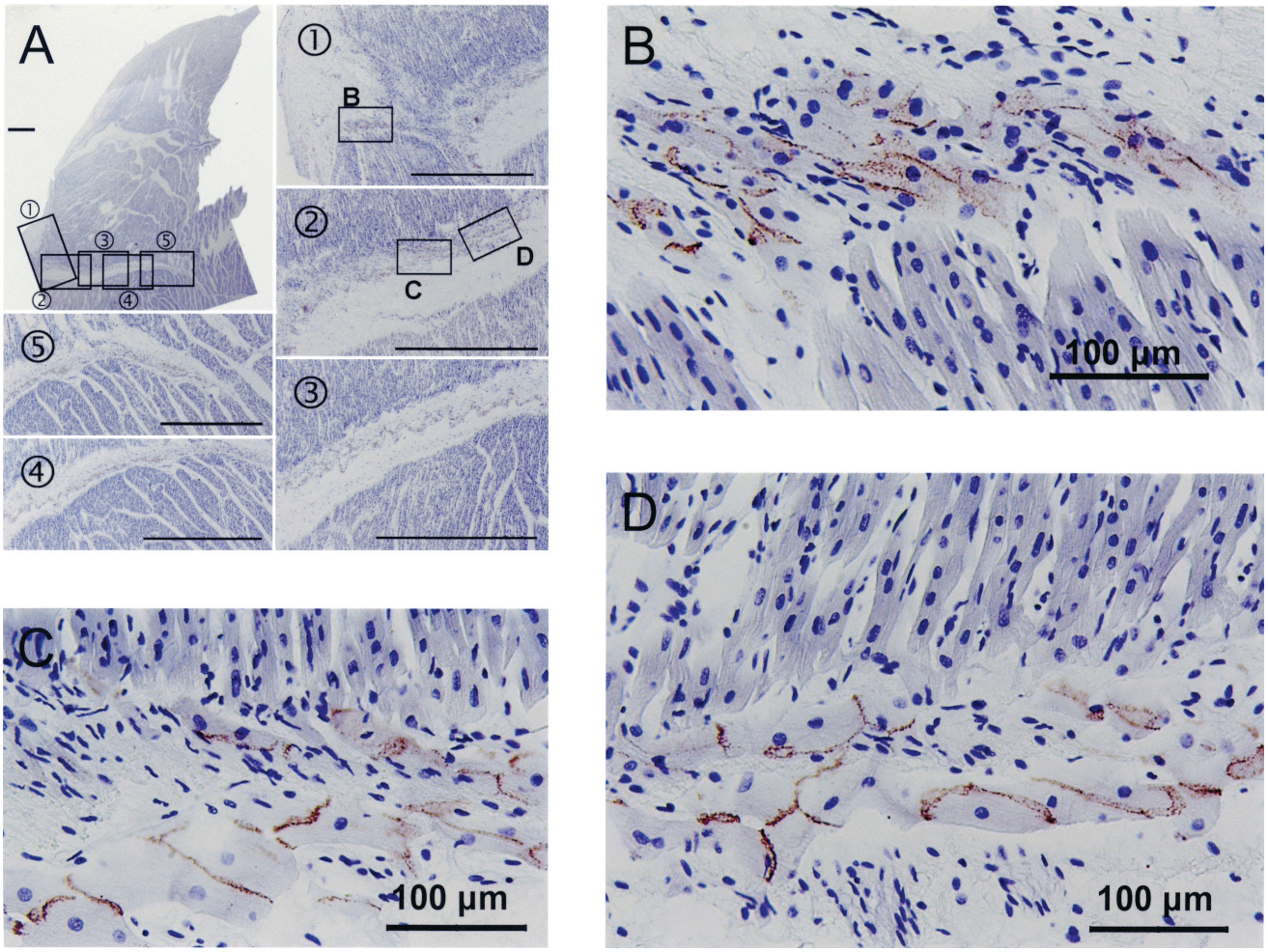

Figure 6. Intramyocardial Purkinje fibers and PVJs at the base of the PM in LV shown by Cx40 immunostaining. A, Low-power image of PM with a Purkinje fiber at its base. Boxes 1 through 5 refer to higher-power images of the Purkinje fiber along its course. Bars=1 mm. Boxes C and D correspond with panels C and D of this figure. B, Multiple PVJs at the muscle bundle below PM (see box in panel A1). C and D, Multiple PVJs at the PM base (see boxes in panel A2).

deterministic. A given tissue could exhibit different reentrant patterns in different episodes (Figures 2 and 3). While reentry occurred at these sites, it was still unstable. The mechanism for this instability was most often interference by other wavelets. Thus, these anatomic patterns seemed to play a facilitator role in the occurrence of reentry that was insufficient to completely stabilize it in our multiple-wavelet VF model.

Reentry Frequency, VF Frequency, Frequency Domains, and Anatomic Structure

A significant correlation between reentry frequency and the dominant frequency of VF was found (Figure 7).[8] Transmural frequency mapping revealed organized regions of similar frequencies (frequency domains). In contrast with previous descriptions,[9] the spatial distribution of individual frequencies was unstable over time in a given tissue over different acquisitions. However, the specific activation patterns, including the occurrence of reentry, impacted significantly on the specific domain localization. Figure 7 shows how, for a given tissue, the domains' spatial location changed over time. Different reentrant patterns occurred in a given tissue in different VF episodes (isochronal maps in panels B and D for the same RV tissue as in Figures 2 and 3 and in panels F and H for the same tissue as in Figure 4). The dominant frequency maps were completely different each episode. The frequency domains existed irrespective of the presence or absence of detectable reentry (panel K). The location of some frequency domain boundaries was stationary over time. This was most obvious in the PM insertion; in 82% (36 of 44) and 78% (21 of 27) of the VF episodes in RV and LV, respectively, a frequency domain boundary could be localized to the PM. Figure 7 shows examples (dotted red line in panels A, C, E, G, I, K, and L). Stationary boundaries were also seen at sites of tissue heterogeneity (such as those where reentry localized), as shown in Figures 5S and 5T. No significant consistent epicardial-to-endocardial frequency gradient was found.

Discussion

The major findings of this study are the following: (1) the demonstration and characterization of both intramural and transmural reentry during VF in isolated swine ventricles and (2) the demonstration of the impact of anatomic structures on

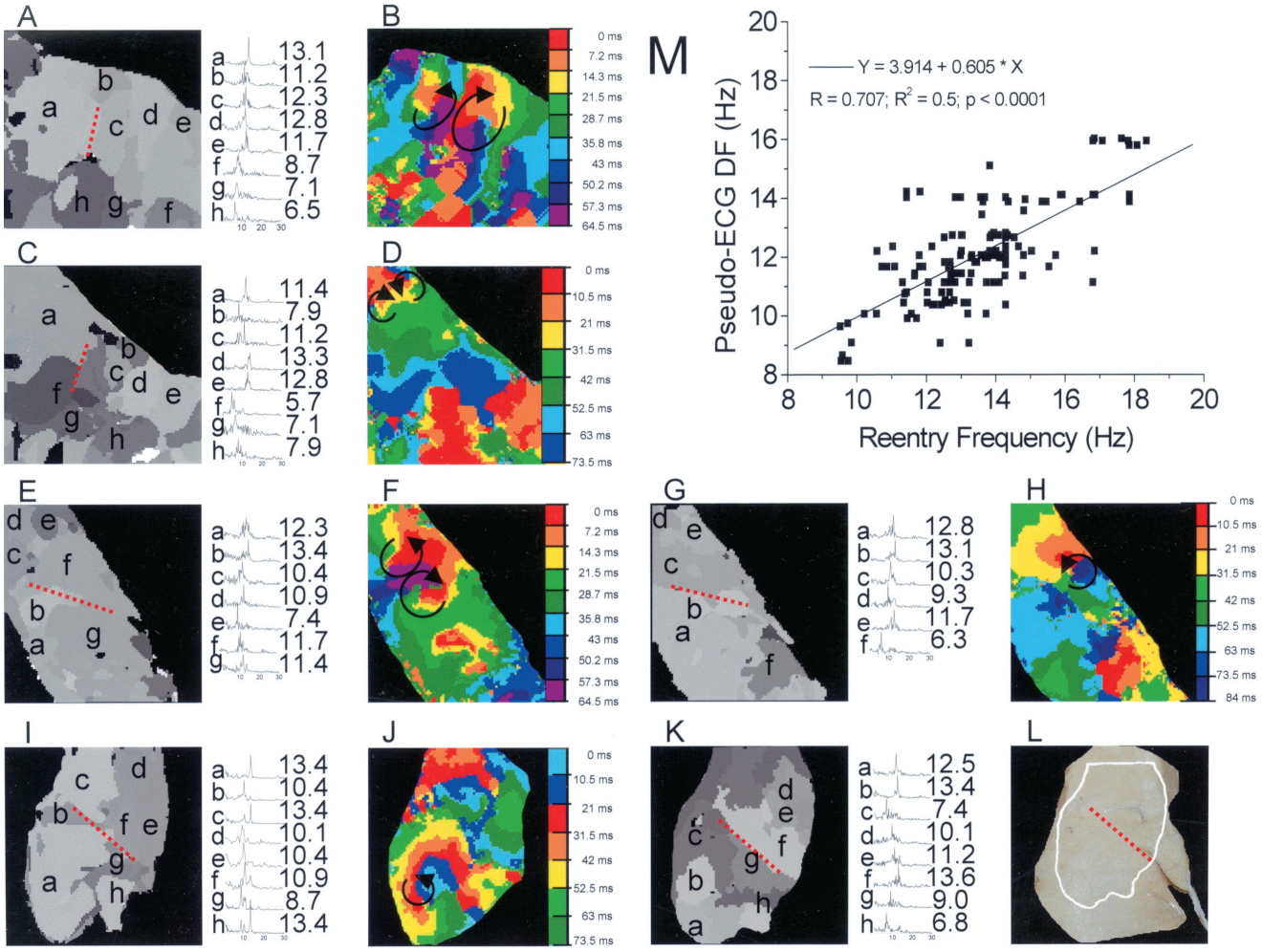

Figure 7. Unstable frequency domains during VF. Panels A through D derive from the same tissue as Figures 2 and 3. A and C, Frequency maps during VF episodes that contained the reentry for which isochronal maps are shown in panels B and D. Red dashed line marks a stable domain boundary that outlined the PM (see panels K and I in Figures 2 and 3). E through H, Two different VF episodes in LV (same tissue as in Figure 4), containing 2 different reentrant patterns (isochronal maps in panels F and H), and 2 frequency maps that, although different, show a persistent boundary in the location of the PM root (red dashed line and Figure 4I). I through L, Frequency maps during VF containing an episode of reentry (panel I, and isochronal map in panel J) and without mapped reentry (K). Frequency domains exist without mappable reentry. A boundary persists in the PM root (red dashed line in panels I, K, and L). M, Correlation between reentry frequency (abscissa) and VF pseudo-ECG dominant frequency (ordinate).

wavelet behavior. Reentry was mostly short-lived, but it could also last for a long time (47 cycles in RV and 54 cycles in LV). In the RV, transmural reentry was common, and the reentrant pathway often included subendocardial structures such as the PM root and trabeculae. True intramural reentry was rare in the RV. In contrast, all reentrant episodes in LV were intramural. Reentry and wave splitting tended to occur around the PM or in areas with anisotropy (abrupt changes in fiber orientation). The intramyocardial Purkinje system may play a role in the generation of reentry.

Intramural Reentry and the Mechanism of VF

On the basis of frequency analysis, recent investigations have suggested the presence of high-frequency periodic sources underlying VF.[8] The nature of these sources has been hypothesized to be reentrant on the basis of the facts that the few visualized episodes of reentry had the same frequency as the dominant frequency and that such high frequencies cannot be accounted for by the known mechanisms of automaticity.[8,9] Because the dominant frequency is also present in cases of repetitive breakthrough activations, which are the most frequent form of periodicity,[6–8] it has been inferred that intramural reentry underlies most of these cases. Further conceptual support for this hypothesis is provided by theoretical studies in which 3-dimensional reentry inside the myocardial wall seems to be organized so that it rotates around the long axis of the myocardial fibers.[22] Moreover, it has been demonstrated that the spatial distribution of the dominant frequencies is relatively simple and stationary over time.[9] These considerations would suggest that continuous, spatiotemporally stable intramural reentry underlies VF and therefore should be necessary for VF to be sustained. Although demonstration of intramural reentry has been reported,[12,13] it is unclear whether or not intramural reentry is required to sustain VF.

Our results show that intramural or transmural reentry is indeed present. Because some of these episodes might last >40 cycles, it is possible that these reentrant wavelets could serve as a source of rapid activation during VF. However, the vast majority of these reentrant wavelets were spatiotemporally unstable. Long-lasting intramural reentry was an exception rather than a rule. Occasionally we observed VF in the absence of any transmural or intramural reentry. These episodes suggest that either we have failed to detect the focal source (the mother rotor) or sustained reentry is not important to the mechanisms of VF. Therefore, the observations of the present study are compatible with both the focal-source hypothesis[23] and the multiple-wavelet hypothesis[24] of cardiac fibrillation.

Many previous studies[1,4,6–8,25] have documented the presence of epicardial or endocardial reentry during VF. The overall incidence of transmural reentry reported in the present study only slightly exceeded the incidence of epicardial or endocardial reentry reported in those communications. Lee et al[4] reported that per 4 seconds of VF, there were on average 1.2 episodes of reentry, with a cycle length of 111 ms and lasting 3.4 rotations. Therefore, in 452 ms out of the 4 seconds (11.3%), organized reentry was present on the epicardium in canine VF. Rogers et al[25] reported that 2.3% of the activation pathways during epicardial VF mapping were unequivocally reentrant and suggested that an additional 28% could also have been so by scaling analysis. We found that 15% and 23% of the visualized wavelets were reentrant in the RV and the LV, respectively.

Tissue Heterogeneity, Intramyocardial Purkinje Fibers, and Wavelet Behavior

In accord with previous work, remarkable relationship between tissue structure and wavelet behavior was found in this study. Microscopic[26] and macroscopic[2,27–31] heterogeneities, whether they are natural,[2,27,29,30] artificially created,[28,31,32] or the result of a pathological process,[33] significantly affect wavelet behavior, creating conduction delays or blocks and facilitating wavelet anchoring. Their impact in multiple-wavelet VF is not completely deterministic, but transient anchoring can be induced.[31] Nonrandom spatial localization of reentry has been described in epicardial VF mapping,[25] but no attempts were made to anatomically characterize the sites of reentry. Our results suggest that certain anatomic patterns—associated or not with macroscopic structures—can increase the likelihood of reentry at their locations.

We also describe wave splitting as a frequent consequence of anisotropy that could have arisen from fiber orientation heterogeneities. Areas of excessive curvature can lead to conduction failure,[34] but at the same time, adjacent areas with lesser curvature could also lead to wavelet attachment,[28] which could explain the occurrence of both phenomena, given the dynamic nature of VF.

The Purkinje system could have contributed significantly to our results. The localization of PVJ at the base of the PM has been documented functionally.[20] We extend these findings with the description of intramyocardial PVJs deep into the root of the PM (Figure 6). A propensity for unidirectional conduction block at the PVJs has been well described in pacing studies.[18,19,35] This block sets the stage for Purkinje-muscle reentrant excitation,[36] which has been recently implicated as a mechanism of polymorphic ventricular arrhythmias in simulation studies.[37] Our data suggest that both conduction block (leading to wave splitting) and reentry at the PM root could have had the participation of PVJ, further confirming the relevance of the Purkinje system during VF. Furthermore, the localization of intramyocardial or transitional Purkinje fibers in between muscle bundles (specifically endocardial trabeculae; see online Figure 3 in the data supplement [http://www.circresaha.org]) may potentially have impaired conduction leading to wave splitting at other locations as well.

Anatomic heterogeneities have been speculated to underlie the complex spatial distribution of excitation frequencies.[9] We show a direct spatial correlation between some domain boundaries and anatomic heterogeneities (Figures 5 and 7), confirming this hypothesis. However, in contrast with recent observations,[9] we found no temporal stability of the frequency domains during VF.

Technical Limitations

Both our in vitro models are isolated, cut portions of ventricular tissue, and our results may not apply directly to the behavior of VF in vivo. By cutting and exposing the myocardial wall, new boundaries were generated that might have impacted on wavelet behavior. Although our study provides insight into the 3-dimensional dynamics of VF, our methods are still 2-dimensional and therefore limited to the mapped transmural surface.

Implications

In this study we show that anatomic structures and myocardial anisotropy played key roles in the generation of wave splitting and in the maintenance of intramural and transmural reentry in normal swine ventricles. Disease states, such as myocardial infarction, may further increase structural abnormality and promote arrhythmogenesis through similar mechanisms.[33]

Acknowledgments

This study was supported by a Postdoctoral Fellowship Award from the American Heart Association, Western States Affiliate (to M.V.), a Cedars-Sinai ECHO Foundation Award (to H.S.K.), a Pauline and Harold Price Endowment (to P.-S.C), an NIH Specialized Center of Research Grant in Sudden Death (Grant P50-HL-52319), NIH Grant R01 HL-66389, AHA National Center Grants-in-Aid (Grants 9750623N and 9950464N), and the Ralph M. Parsons Foundation. We thank Dr Ali Hamzei, Elaine Lebowitz, and Avile McCullen for assistance.

References

1. Chen P-S, Wolf PD, Melnick SD, Danieley ND, Smith WM, Ideker RE. Comparison of activation during ventricular fibrillation and following unsuccessful defibrillation shocks in open chest dogs. *Circ Res*. 1990;66:1544–1560.
2. Davidenko JM, Pertsov AM, Salomonsz R, Baxter W, Jalife J. Stationary and drifting spiral waves of excitation in isolated cardiac tissue. *Nature*. 1992;355:349–351.
3. Gray RA, Jalife J, Panfilov AV, Baxter WT, Cabo C, Davidenko JM, Pertsov AM, Hogeweg P. Mechanisms of cardiac fibrillation. *Science*. 1995;270:1222–1223.

4. Lee JJ, Kamjoo K, Hough D, Hwang C, Fan W, Fishbein MC, Bonometti C, Ikeda T, Karagueuzian HS, Chen P-S. Reentrant wave fronts in Wiggers' stage II ventricular fibrillation: characteristics, and mechanisms of termination and spontaneous regeneration. *Circ Res*. 1996;78: 660–675.
5. Janse MJ, Wilms-Schopman FJ, Coronel R. Ventricular fibrillation is not always due to multiple wavelet reentry. *J Cardiovasc Electrophysiol*. 1995;6:512–521.
6. Witkowski FX, Leon LJ, Penkoske PA, Giles WR, Spano ML, Ditto WL, Winfree AT. Spatiotemporal evolution of ventricular fibrillation. *Nature*. 1998;392:78–82.
7. Gray RA, Pertsov AM, Jalife J. Spatial and temporal organization during cardiac fibrillation. *Nature*. 1998;392:75–78.
8. Chen J, Mandapati R, Berenfeld O, Skanes AC, Jalife J. High-frequency periodic sources underlie ventricular fibrillation in the isolated rabbit heart. *Circ Res*. 2000;86:86–93.
9. Zaitsev AV, Berenfeld O, Mironov SF, Jalife J, Pertsov AM. Distribution of excitation frequencies on the epicardial and endocardial surfaces of fibrillating ventricular wall of the sheep heart. *Circ Res*. 2000;86: 408–417.
10. Chen P-S, Wolf PD, Dixon EG, Danieley ND, Frazier DW, Smith WM, Ideker RE. Mechanism of ventricular vulnerability to single premature stimuli in open-chest dogs. *Circ Res*. 1988;62:1191–1209.
11. Frazier DW, Wolf PD, Wharton JM, Tang ASL, Smith WM, Ideker RE. Stimulus-induced critical point: mechanism for electrical initiation of reentry in normal canine myocardium. *J Clin Invest*. 1989;83:1039–1052.
12. Pogwizd SM, Corr PB. Reentrant and nonreentrant mechanisms contribute to arrhythmogenesis during early myocardial ischemia: results using three-dimensional mapping. *Circ Res*. 1987;61:352–371.
13. Baxter WT, Mironov SF, Zaitsev AV, Jalife J, Pertsov AM. Visualizing excitation waves inside cardiac muscle using transillumination. *Biophys J*. 2001;80:516–530.
14. Kim Y-H, Garfinkel A, Ikeda T, Wu T-J, Athill CA, Weiss JN, Karagueuzian HS, Chen P-S. Spatiotemporal complexity of ventricular fibrillation revealed by tissue mass reduction in isolated swine right ventricle: further evidence for the quasiperiodic route to chaos hypothesis. *J Clin Invest*. 1997;100:2486–2500.
15. Yan GX, Shimizu W, Antzelevitch C. Characteristics and distribution of M cells in arterially perfused canine left ventricular wedge preparations. *Circulation*. 1998;98:1921–1927.
16. Voroshilovsky O, Qu Z, Lee M-H, Ohara T, Fishbein GA, Huang H-LA, Swerdlow CD, Garfinkel A, Weiss JN, Karagueuzian HS, Chen P-S. Mechanisms of ventricular fibrillation induction by 60 Hz alternating current in isolated swine right ventricle. *Circulation*. 2000;102: 1569–1574.
17. Gros D, Jarry-Guichard T, Ten Velde I, de Maziere A, van Kempen MJ, Davoust J, Briand JP, Moorman AF, Jongsman HJ. Restricted distribution of connexin40, a gap junctional protein, in mammalian heart. *Circ Res*. 1994;74:839–851.
18. Mendez C, Mueller WJ, Urguiaga X. Propagation of impulses across the Purkinje fiber-muscle junctions in the dog heart. *Circ Res*. 1970;26: 135–150.
19. Overholt ED, Joyner RW, Veenstra RD, Rawling D, Wiedmann R. Unidirectional block between Purkinje and ventricular layers of papillary muscles. *Am J Physiol*. 1984;247:H584–H595.
20. Myerburg RJ, Nilsson K, Gelband H. Physiology of canine intraventricular conduction and endocardial excitation. *Circ Res*. 1972;30:217–243.
21. Tranum-Jensen J, Wilde AA, Vermeulen JT, Janse MJ. Morphology of electrophysiologically identified junctions between Purkinje fibers and ventricular muscle in rabbit and pig hearts. *Circ Res*. 1991;69:429–437.
22. Berenfeld O, Pertsov AM. Dynamics of intramural scroll waves in three-dimensional continuous myocardium with rotational anisotropy. *J Theor Biol*. 1999;199:383–394.
23. Jalife J, Berenfeld O, Skanes A, Mandapati R. Mechanisms of atrial fibrillation: mother rotors or multiple daughter wavelets, or both? *J Cardiovasc Electrophysiol*. 1998;9(suppl 8):S2–S12.
24. Moe GK, Rheinboldt WL, Abildskov JA. A computer model of atrial fibrillation. *Am Heart J*. 1964;64:200–220.
25. Rogers JM, Huang J, Smith WM, Ideker RE. Incidence, evolution, and spatial distribution of functional reentry during ventricular fibrillation in pigs. *Circ Res*. 1999;84:945–954.
26. Spach MS, Dolber PC. Relating extracellular potentials and their derivatives to anisotropic propagation at a microscopic level in human cardiac muscle: evidence for electrical uncoupling of side-to-side fiber connections with increasing age. *Circ Res*. 1986;58:356–371.
27. Pertsov AM, Davidenko JM, Salomonsz R, Baxter WT, Jalife J. Spiral waves of excitation underlie reentrant activity in isolated cardiac muscle. *Circ Res*. 1993;72:631–650.
28. Ikeda T, Yashima M, Uchida T, Hough D, Fishbein MC, Mandel WJ, Chen P-S, Karagueuzian HS. Attachment of meandering reentrant wave fronts to anatomic obstacles in the atrium: role of the obstacle size. *Circ Res*. 1997;81:753–764.
29. Wu T-J, Yashima M, Xie F, Athill CA, Kim Y-H, Fishbein MC, Qu Z, Garfinkel A, Weiss JN, Karagueuzian HS, Chen P-S. Role of pectinate muscle bundles in the generation and maintenance of intra-atrial reentry: potential implications for the mechanism of conversion between atrial fibrillation and atrial flutter. *Circ Res*. 1998;83:448–462.
30. Kim Y-H, Xie F, Yashima M, Wu T-J, Valderrábano M, Lee M-H, Ohara T, Voroshilovsky O, Doshi RN, Fishbein MC, Qu Z, Garfinkel A, Weiss JN, Karagueuzian HS, Chen P-S. Role of papillary muscle in the generation and maintenance of reentry during ventricular tachycardia and fibrillation in isolated swine right ventricle. *Circulation*. 1999;100: 1450–1459.
31. Valderrábano M, Kim Y-H, Yashima M, Wu T-J, Karagueuzian H, Chen P-S. Obstacle-induced transition from ventricular fibrillation to tachycardia in isolated swine right ventricles: insights into the transition dynamics and implications for the critical mass. *J Am Coll Cardiol*. 2000;36:2000–2008.
32. Xie F, Qu Z, Garfinkel A. Dynamics of reentry around a circular obstacle in cardiac tissue. *Physiol Rev E*. 1998;58:6355–6358.
33. Peters NS, Coromilas J, Severs NJ, Wit AL. Disturbed connexin43 gap junction distribution correlates with the location of reentrant circuits in the epicardial border zone of healing canine infarcts that cause ventricular tachycardia. *Circulation*. 1997;95:988–996.
34. Cabo C, Pertsov AM, Baxter WT, Davidenko JM, Gray RA, Jalife J. Wavefront curvature as a cause of slow conduction and block in isolated cardiac muscle. *Circ Res*. 1994;75:1014–1028.
35. Gilmour RF, Davis JR, Zipes DP. Overdrive suppression of conduction at the canine Purkinje-muscle junction. *Circ Res*. 1987;76:1388–1396.
36. Sasyniuk B, Mendez C. A mechanism for reentry in canine ventricular tissue. *Circ Res*. 1971;28:3–15.
37. Berenfeld O, Jalife J. Purkinje-muscle reentry as a mechanism of polymorphic ventricular arrhythmias in a 3-dimensional model of the ventricles. *Circ Res*. 1998;82:1063–1077.

Dynamics of Intramural and Transmural Reentry During Ventricular Fibrillation in Isolated Swine Ventricles

On-line data supplement.

Methods.

The experimental protocol was approved by the Institutional Animal Care and Use Committee at the Cedars-Sinai Medical Center and conforms to the guidelines established by the American Heart Association.

RV preparation

The experimental model has been previously described.[1] Briefly, the hearts of 9 farm pigs of either sex (25 to 32 kg) were used for the study. After the hearts were extracted, the right coronary artery was perfused with oxygenated Tyrode's solution. The composition of the Tyrode's solution was as follows (mM): NaCl, 125; KCl, 4.5; $MgCl_2$, 0.5; $CaCl_2$, 0.54; NaH_2PO_4, 1.2; $NaHCO_3$, 24; and glucose, 5.5, along with albumin 50mg/L. The RV wall (weighting 28.3 to 34.6 g) was then excised and placed in a tissue bath, with the endocardium facing up. VF, which occurred during tissue manipulation, persisted in vitro in the isolated RV. An oblique cut was then performed at the distal edge, exposing the transmural surface (see Figure 1). The cut was performed so that it would include the papillary muscle (PM). Optical mapping (see below) was performed in the cut surface as well as the adjacent endocardial surface.

LV preparation

While experiments were conducted with RV, the LV was preserved by infusion of ice-cold cardioplegic solution (St Thomas's Hospital).[2] The composition of this solution was as follows (mM): NaCl, 110; KCl, 16; $MgCl_2$, 16; $CaCl_2$, 1.2; $NaHCO_3$, 10; with a pH of 7.8. A 3-minute infusion was performed every 20 minutes[2] through a cannula into the left main coronary artery. Our LV wedge preparation was similar to that developed in Antzelevitch's laboratory.[3] In 4 tissues, the proximal left anterior descending coronary artery, the ramus intermedius (if present) and the first obtuse marginal arteries were ligated. A rim of tissue surrounding the left circumflex and the second obtuse marginal artery was excised, leaving an inverted L-shaped preparation (see Figure 1) that always contained at least part of the posteromedial PM. The angle formed by the obtuse marginal and circumflex arteries was opened and the tissue was placed in the tissue bath with the transmural cut surface up, allowing mapping studies. In 2 tissues, the left circumflex artery was ligated proximally and a wedge of tissue surrounding the left anterior descending artery was cut, exposing the transmural surface of the interventricular septum. Once the tissue was cut, warm, oxygenated Tyrode's solution was substituted for the cardioplegic solution. Six out of 9 tissues developed VF after rewarming. VF persisted in these tissues for 63 to 79 minutes. These six LV wedges (weighting 37.6 to 42.8 g) were used for the experiments.

Optical Mapping

The optical mapping system was similar to the one described previously.[4] The tissues were stained for 20 minutes with 1 to 2 μmol/L di-4-ANEPPS (Molecular Probes,

Inc) in the Tyrode's solution. The tissue was illuminated quasi-monochromatic light (500±30 nm) from a 250 W tungsten-halogen lamp (Model 66196, Oriel Corp, Stratford, CT). The induced fluorescence was collected through a 600 nm long-pass glass filter (R60, Nikon, Tokyo, Japan) and a 25 mm/f-stop 0.85 video lens (Fujinon CF25L, Fuji Photo Optical Co., Omiya City, Japan) with a 12-bit CCD camera (Dalsa Inc, Ontario, Canada) operating at ≈ 279 frames per second (3.58 ms sampling interval) acquiring 96 x 96 sites simultaneously over a 35 x 35 mm^2 area, resulting in a spatial resolution of 0.36 x 0.36 mm^2 per pixel. Each acquisition lasted for 4.3 s. The digital images were transferred to a personal computer with a frame grabber (IC-PCI-DIG16, Imaging Technology, Bedford, MA). No electromechanical uncouplers were used in the study.

Data Analysis

The optical signals were temporally filtered and spatially averaged to reduce noise.[4] For temporal filtering, we applied a 5-point time median filter to each pixel. We took the original first 5 data points (let's call them frames 1,2,3,4,5), found the median value of those points and used that as the new value for point (frame) 3. Then we took the next original 5 points (i.e. frames 2,3,4,5,6), found the median value of those and use that as the new value for point 4. We continued this exercise until the end of the data. We then took the tracing, inverted the data, and brought the baseline down to zero, which was defined by the average of the 5 lowest fluorescent values recorded by that pixel. Afterwards we range-normalized each pixel: we found the 5 lowest and 5 highest points and took the average of those numbers. Then we adjusted each pixel's fluorescent value by the same amount so that the highest pixel value would be 255 and the lowest would be

0. Next, for each pixel on the frame, we averaged the fluorescent values of the pixel and its 8 surrounding pixels. We used this average as the new value for the pixel. At completion of those averaging procedures, we repeated the procedure for a second time. At that time we re-zeroed the signal by bringing the baseline down to zero, defined by the average of the 5 lowest points of each pixel. We then range-normalized the signals again. The maximal signal amplitude was coded white, representing fully depolarized state. The minimum signal amplitude was coded black, representing fully repolarized state. Each pixel was then assigned a shade of gray between white and black.

The activation wavelets were detected as follows: the computer first detected every adjacent pair of pixels in the frame that crossed the normalized median value of the data and generated a line in between them; if the intensity of the data on which the line coincided increased over time (as determined by regression analysis), that edge was identified as the activation wavefront and colored red. Otherwise, if the intensity decreased, the edge was identified as the repolarization waveback and colored green. The area between a red and a green line constituted a wavelet. We defined a *wavebreak point* in a propagating wavelet as a point where the activation wavefront (red line) and the repolarization waveback (green line) met. This term and definition were chosen instead of *phase singularity point*[5] since completion of a full reentrant rotation around it was not required. Wave splitting was defined as the generation of two daughter wavelets –and two wavebreak points- from a single wavelet. Reentry was defined to be present when a wavefront rotated clockwise or counterclockwise around a wavebreak point completing a 360° cycle. Reentry was considered intramural when the complete rotation occurred within the wall without invading the adjacent endocardial or epicardial surface.

Conversely, transmural reentry was defined as that which involved both the myocardial wall and the endocardium or subendocardial structures such as the PM or trabeculae for complete reentrant excitation. Anchoring was defined as the occurrence of reentry in a fixed anatomical location for 2 or more cycles. The fraction of reentrant wavelets was determined by the ratio of the number of wavelets participating in a reentrant circuit over the total number of wavelets in the mapping field. Wavelets that were small (less than 8 pixels), discontinuous (mosaic-like pattern), or inconsistent over time (not present in subsequent acquisition frames) were not counted as such.

We also generated isochronal maps based on the location of wavefronts at each frame. First, we selected a start frame and an end frame. Second, we selected how many frames should be assigned to each isochrone. In this study, we chose 2 or 3 frames. Third, the program identified the location of the activation wavefronts in these chosen frames and assigned a different color to each of them. The areas between the colored lines were also colored.

Data are reported as mean ± standard deviation. Simple linear regression analysis was used to correlate frequencies. Student's *t* test was used to compare means. Chi-square test was used to compare the proportion of reentrant episodes in LV versus RV as well as the proportion of reentrant episodes anchoring to the PM. A p value ≤ 0.05 was considered significant.

Histological and Immunohistochemical Studies

After the study, the LV and RV were fixed with 4% formalin for one hour, followed by preservation in 70% alcohol.[6] Transmural sections of 5 μm were cut parallel

to the mapped surface from a paraffin-embedded tissue block and stained with Masson's trichrome. Fiber orientation patterns were correlated with activation patterns visualized by optical mapping. All sites of reentry anchoring and wave splitting were correlated with local histological patterns.

In an attempt to demonstrate intramyocadial Purkinje fibers, we used connexin 40 (Cx40) immunostaining.[7] For these immunohistochemical studies, the tissue slides were deparaffinized and rehydrated using a graded xylene and alcohol series. The slides were then reacted with 3% hydrogen peroxide to inactivate endogenous peroxidase. Sections were incubated with rabbit anti-mouse Cx40 antibody (Alpha diagnostic, San Antonio, TX). The slides were then incubated with peroxidase-conjugated streptavidin (DAKO Corp) for 30 min. Sections were washed with PBS between each step and all procedures were performed in a humidified chamber at room temperature. The immunoreactive products were visualized through incubation of tissue section for 2 to 3 minutes with DAKO Liquid Substrate-Chromogen System. The sections were then counterstained with hematoxylin, rinsed with an acid/alcohol solution for 3 seconds, dehydrated through a graded alcohol series, and mounted.

Electrocardiographic and Frequency Analysis

A whole-tissue ECG was recorded using two hook electrodes positioned at each edge of the tissue (labeled "pseudo-ECG" in Figure 1), at a sampling rate of 2400 Hz. Fast Fourier Transformation (FFT) was performed using Origin 5.0 software (Microcal, Northampton, MA), on signals from the recorded global ECG, as well as on the local fluorescence signals from each pixel of the optical mapping field. The dominant

frequency (DF) was defined as that with the highest power of each frequency spectrum. Frequency domain maps were constructed as previously reported.[8]

Online Figure 1. The experimental setup. A, isolated RV with an oblique cut at the edge. B, LV wedge including the circumflex and second obtuse marginal arteries. The angle between arteries (curved arrow) was opened to expose the transmural surface. C and D, schematic representation of the RV and LV experimental setup, respectively.

Online Figure 2. Intramural reentry in the RV. A through G, one cycle of intramural reentry (white arrows). H, schematic of the reentrant circuit (the dotted red line shows the endocardial edge of the transmural cut surface), and the location of the channels whose optical action potentials are shown in K (in fluorescence –F- units). I, histology at the site of wave splitting at the PM root. Black bar marks 1mm scale. J, isochronal map.

Online Figure 3. Endocardial trabecula separated from the RV by an intramyocardial Purkinje fiber. A, low power image of the trabecula. Boxes locate the higher-power images in panels B, C, and D. Connexin 40 immunostaining (brown color in the intercellular junctions) demonstrates intramyocardial Purkinje fibers.

References

1. Kim Y-H, Garfinkel A, Ikeda T, Wu T-J, Athill CA, Weiss JN, Karagueuzian HS, Chen P-S. Spatiotemporal complexity of ventricular fibrillation revealed by tissue mass reduction in isolated swine right ventricle. Further evidence for the quasiperiodic route to chaos hypothesis. *J Clin Invest.* 1997;100:2486-2500.
2. Ledingham SJM, Braimbridge MV, Hearse DJ. The St. Thomas' Hospital cardioplegic solution. A comparison of the efficacy of two formulations. *J Thorac Cardiovasc Surg.* 1987;93:240-246.
3. Yan GX, Shimizu W, Antzelevitch C. Characteristics and distribution of M cells in arterially perfused canine left ventricular wedge preparations. *Circulation.* 1998;98:1921-1927.
4. Voroshilovsky O, Qu Z, Lee M-H, Ohara T, Fishbein GA, Huang H-LA, Swerdlow CD, Garfinkel A, Weiss JN, Karagueuzian HS, Chen P-S. Mechanisms of ventricular fibrillation induction by 60 Hz alternating current in isolated swine right ventricle. *Circulation.* 2000;102:1569-1574.
5. Gray RA, Pertsov AM, Jalife J. Spatial and temporal organization during cardiac fibrillation. *Nature.* 1998;392:75-78.
6. Cao J-M, Chen LS, Kenknight BH, Ohara T, Lee M-H, Tsai J, Lai WW, Karagueuzian HS, Wolf PL, Fishbein MC, Chen P-S. Nerve sprouting and sudden cardiac death. *Circ Res.* 2000;86:816-821.
7. Gros D, Jarry-Guichard T, Ten Velde I, de Maziere A, van Kempen MJ, Davoust J, Briand JP, Moorman AF, Jongsman HJ. Restricted distribution of connexin40, a gap junctinal protein, in mammalian heart. *Circ Res.* 1994;74:839-851.

8. Zaitsev AV, Berenfeld O, Mironov SF, Jalife J, Pertsov AM. Distribution of excitation frequencies on the epicardial and endocardial surfaces of fibrillating ventricular wall of the sheep heart. *Circ Res.* 2000;86:408-417.

online figure 1

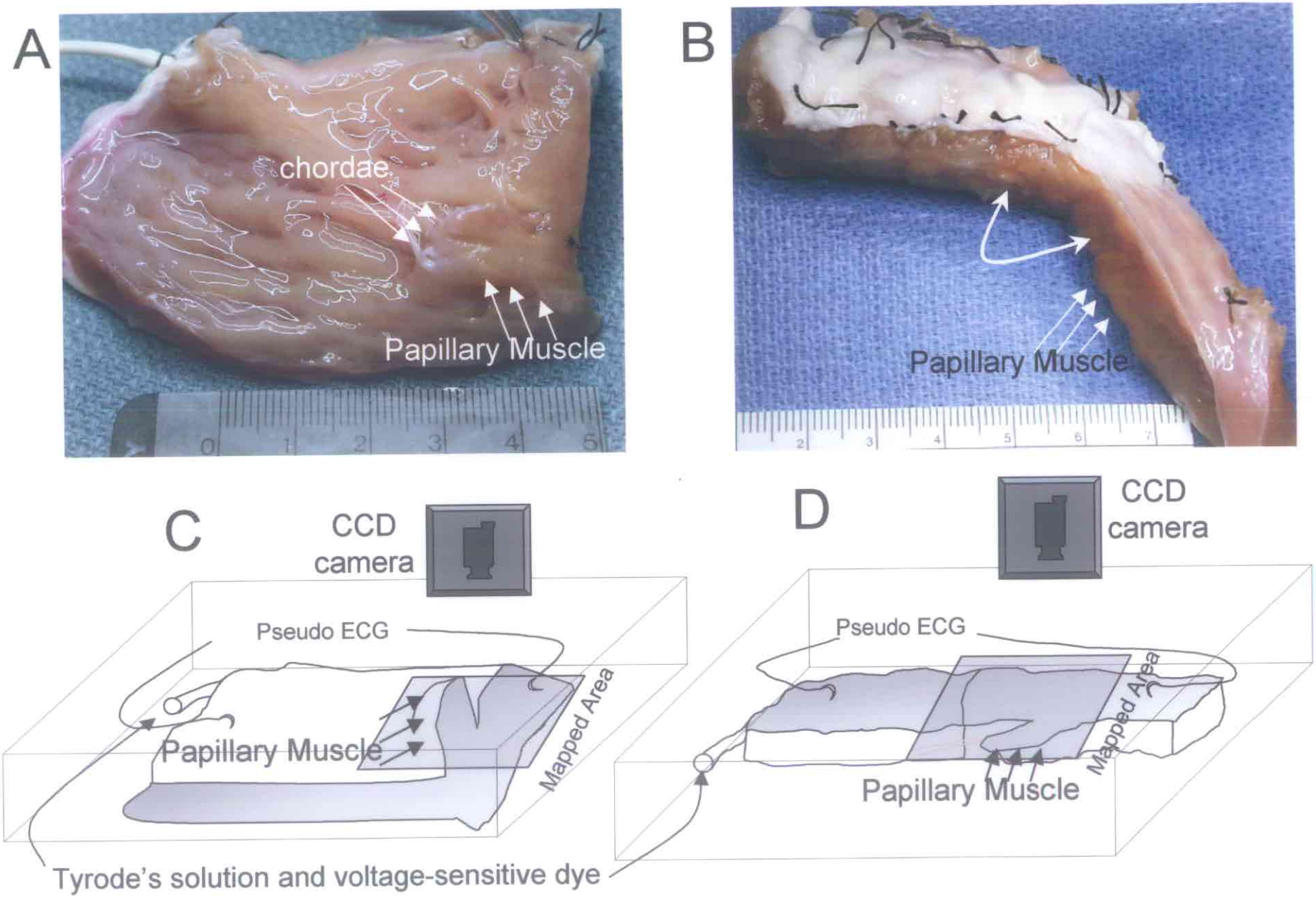

online figure 2

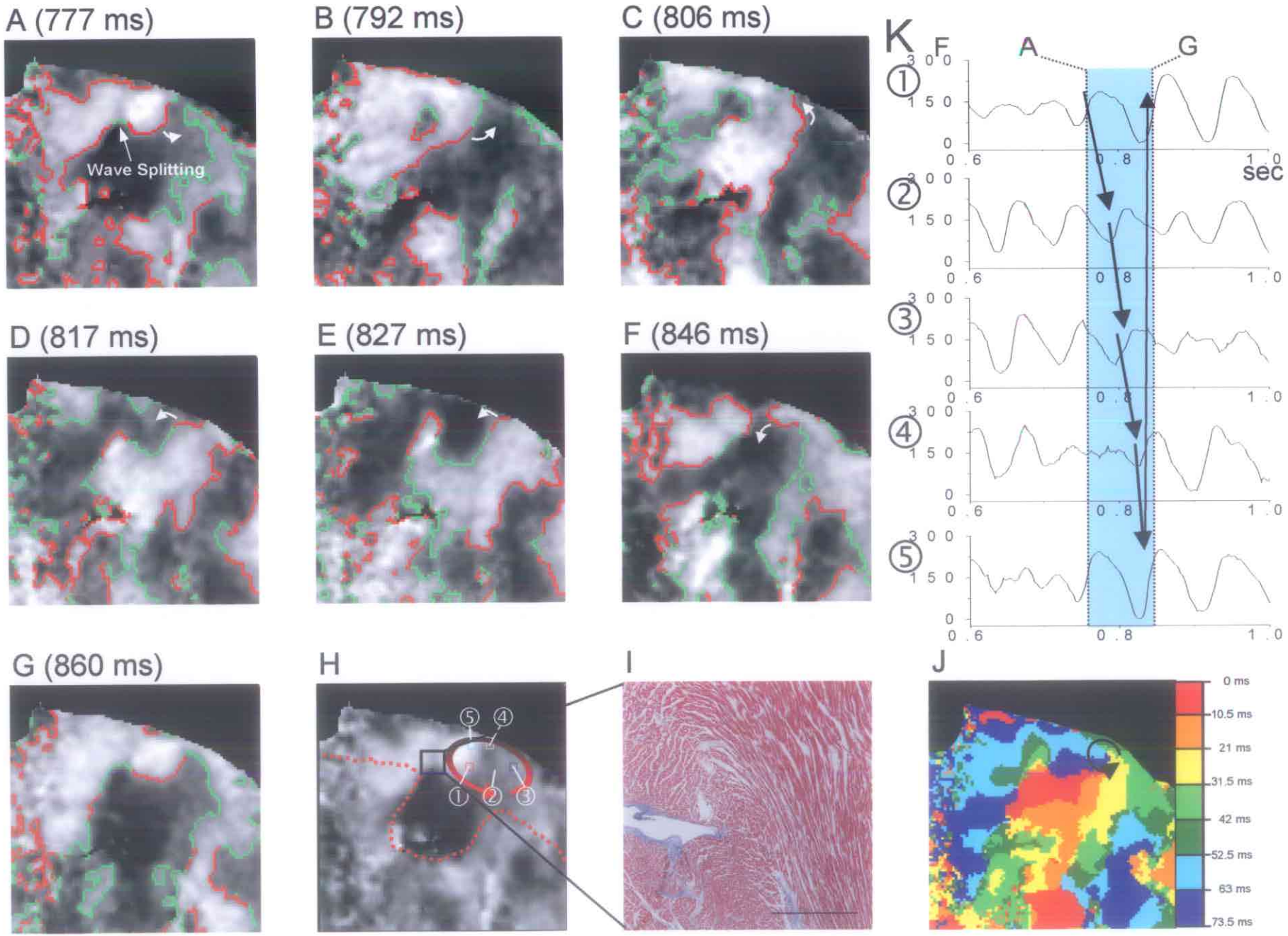

online figure 3